Time-Orthogonal Waveform Diversity and Joint Domain Localised Algorithm for Distributed Aperture Radars

L. Landi R. S. Adve

Abstract

Distributed aperture radars represent an interesting solution for target detection in strong interference environments. Distributed apertures provide improved angular resolution or are able to view a target from multiple look-angles, thereby exploiting scintillation. However, due to the large distances between array elements, both target and interfering sources are in the near field of the antenna array. Furthermore, due to the relative motion between antenna elements and interference sources, the clutter Doppler frequency is not stationary. Recent works have demonstrated the benefits of combining frequency diversity and space time adaptive processing for distributed aperture radars. In this paper a new waveform diversity system model is developed. Using orthogonal signaling, the receivers can treat the incoming signals independently, solving several bistatic problems instead of the initial multistatic problem. We also apply adaptive techniques to counteract the range dependency of the clutter Doppler frequency. In particular, we apply the joint domain localized algorithm, specifically chosen due to its need for only limited secondary data.

1 Introduction

Several works have shown the benefit of the joint use of distributed aperture radars and waveform diversity in conjunction with space-time adaptive processing [1, 2, 3]. *Diversity* is an important issue for many engineering fieds; the most famous schemes are frequency, waveform, time and spatial diversity [4]. While some recent literature has designated this area as multiple-input multiple-output (MIMO) radar [5], we prefer the term 'distributed apertures' keeping in line with prior work in similar radar systems [1]. By using multiple receiving sites the radar is in a multistatic configuration; if in addition multiple transmitting sites are used and their transmissions are coherently phased, so that the transmitters operate as a single transmitting array, the configuration is called distributed aperture radar [6]. The large baseline of the distributed aperture radar results in improved angular resolution compared to the resolution of a monolithic system, at cost of grating lobes or high sidelobes.

The system under consideration here is a very sparse array of sub-apertures placed thousands of wavelengths apart. Each sub-aperture of the array transmits a unique waveform, orthogonal to the signals transmitted by the others; to achieve time orthogonality we use pulses that do not overlap in the time domain. Each aperture receives all the transmitted signals, but, due to the orthogonality assumption, each signal can be treated independent of the others. Furthermore, each transmission is unique in its pulse duration; in this manner waveform diversity among the signals is achieved. The jointly use of distributed aperture radars and waveform diversity leads to a good detection capability, especially due to the high information about the target, and the adaptivity to the scenario due to the waveform diversity. In addition, the time-orthogonality leads to a completely separated signals, making very easy the processing of all of them, and eliminates the cross-talk; the interested reader can find useful related information in [7].

A very important issue arising from the work in [2] and [3] is that, due to the very long baseline, both signals and interference sources are not in the far field of the antenna array. For this configuration, the spatial steering vector depends not only on the signal *angle* of arrival but also on the *distances* between the receivers and target. To take in account this range dependency, some works model the steering vector as a function of the curvature radius of the wave [8], modifying the phase shift contributed to each antenna element. However, as outlined in [2], to exploit waveform diversity for the interesting case

of distributed aperture radars, instead of using phase shifts to model the delay of wave propagation through the array, the processing scheme requires true time delay between the widely distributed antennas. Previous work such as described above has focused on *frequency diversity* to enable orthogonal transmissions from each element in the distributed array. However, frequency diversity raises the difficult issue of coherent processing across a wide frequency range. This paper proposes a system using an alternative approach, based on time orthogonal waveforms with different pulse durations to achieve diversity. Waveform diversity using varying FM rates was proposed in [9] in the context of target tracking. In addition, the distributed radar problem is inherently multistatic with multiple radars illuminating the area of interest, and also receiving and potentially processing all these transmissions. A true development of space-time adaptive processing (STAP) for distributed apertures will therefore include both monostatic [10] and bistatic configurations [11, 12]; from the point of view of one receiving site, the monostatic configuration is due to the signal transmitted by itself, while the bistatic configurations are due to the other transmissions.

In this paper the interference is modeled as a sum of noise and clutter, which is due to a chaff cloud, i.e. a large number of resonant dipoles surrounding the target [13]; the clutter contribution is, in turn, modeled as the sum of several low power interference sources as done for airborne radar in [10]; however, here, each source has a range dependent contribution. A well known problem in bistatic radar [14] is that clutter Doppler center is range dependent due to the relative motion between antennas and interference source. This dependency significantly degrades the achievable performance of the receiver and must be taken in account for effective clutter suppression.

The first goal of this paper is to develop a new model for waveform diversity for distributed aperture radars with time-orthogonal waveforms. In this regard, this paper represents an extension of the available research into waveform diversity for distributed aperture radars and also represents an effort into applying bistatic and multistatic STAP applied to distributed aperture. The time orthogonal waveforms, just like with frequency diversity, allows for independent processing of each transmit-receive combination. However, issues of phase coherence across a wide frequency band are now avoided. In [15] the authors develop waveform diversity using time-overlapping pulses of differing FM rates, however the analysis there is devoted largely to the interaction between the overlapping waveforms. In this paper we introduce a new waveform diversity model that involves the

pulse duration instead of the frequency diversity proposed in [2].

The second goal of this paper is to characterize the impact of clutter non-stationarity due to the bistatic problem in the context of waveform diversity. We analyze the effect of the clutter Doppler frequency non-stationarity and the performance improvement achievable applying specific techniques to counteract it. In particular, we use the *Joint Domain Localized* (JDL) algorithm. The JDL algorithm, first introduced in [16], transforms the received space-time data to the angle-Doppler domain. Adaptive processing is restricted to a localized region centered on the target look point, in the angle-Doppler domain, significantly reducing the degrees of freedom while retaining maximal gain against thermal noise. This in turn reduces the training required for the adaptive processor. Given the inherent non-stationarity of the clutter in distributed aperture systems, this is the primarily motivation to consider reduced rank algorithms such as JDL.

The paper is organized as follows. In Section 2 we introduce the system and interference models without accounting for the range dependency of the clutter. In Section 3 we introduce the problem of the non-stationarity of the environment and illustrate the use of the JDL algorithm as applied to our model. In Section 4 we provide a proof of the CFAR property of the decision statistic considering both the receivers with and without the JDL algorithm. Section 5 presents numerical simulations of the system of interest. In Section 6 we present conclusions and suggest future possible avenues for research.

2 System Model

The system under consideration is a ground based distributed aperture radar attempting to detect low flying targets. The elements of the array are unmoving, widely separated from each others and are placed thousands of wavelengths apart. Given an antenna array of aperture D operating at wavelength λ, the distance r to the far-field must satisfy the following conditions [17]

$$\begin{cases} r & \gg & D, \\ r & \gg & \lambda, \\ r & \gg & 2D^2/\lambda. \end{cases} \tag{1}$$

Using some suggested values for distributed radars, D=200m and λ=0.03m, the far field distance begins at a distance of approximately 2700km. Both target and interference sources are, therefore, in the near-field of the antenna array. In this case the associated steering vectors depend on both angle *and range*, while in the far-field model they depend

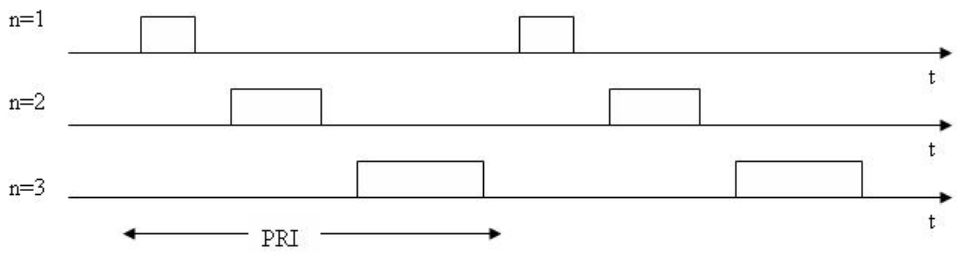

Figure 1: *Time orthogonal signals with different pulse duration and common PRI.*

only on the angle of arrival.

The system is composed of N sub-apertures that are both receivers and transmitters. Each sub-aperture transmits a waveform with a unique pulse width; however, each element receives and processes all transmitted signals. To achieve orthogonality and waveform diversity, the signals do not overlap in the time domain on transmit or receive. Figure 1 presents an example with 3 transmitting elements and 2 pulses per element; in the figure n denotes the transmitting element.

The sensors are located in the (x, y) plane at points $(x_n, y_n), n = 1, \ldots, N$ and transmit a coherent stream of M linear FM pulses, with common frequency f_0, common pulse repetition interval (PRI) T_r, common bandwidth B but different pulse durations, that is, the slope of instantaneous frequency varies among the N transmitted signals. All N elements receive and process all N incoming signals, that is, if M pulses are used in a coherent pulse interval (CPI), the overall return signal over time, space, and waveform can be written as a length-N^2M vector.

Due to the orthogonality of the signals, the receiver processes each incoming signal independently from the others and uses true time delay to focus on a look-point (X_L, Y_L, Z_L). Denote as $D_n = \sqrt{(X_L - x_n)^2 + (Y_L - y_n)^2 + Z_L^2}$ the distance between the look point (where the target is supposed to be) and the n^{th} element. The true time delay used by the receiver i is

$$\Delta T_i = \frac{\max_p\{D_p\} - D_i}{c}, \tag{2}$$

where $p = 1, \ldots, N$ and c is the speed of light. Delaying the signals using this amount means aligning them in the space domain to the furthest element of the array with respect to the look-point; essentially, true time delay nullifies the propagation delay over the array. This also allows for the target to be present in the same range gate for all receive elements. True time delays restore the orthogonality at the receiving sites.

Let us denote by $\mathbf{y}$ the complex vector of the samples from the range cell where the presence of the useful target is sought (primary data). The detection of this target is made difficult by interference comprising thermal noise and clutter. As in [18] we suppose that a target-free secondary data set $\mathbf{y}_k$, $k = 1, \ldots, K$ is available ($K \geq N+1$). The secondary data is assumed homogeneous with respect to the primary data, i.e., the statistics of the interference in both data sets are assumed identical.

The detection problem to be solved can be formulated in terms of the following binary hypotheses test

$$\begin{array}{rcl} H_0 & : & \left\{ \begin{array}{ll} \mathbf{y} & = \mathbf{c} + \mathbf{n} \\ \mathbf{y}_k & = \mathbf{c}_k + \mathbf{n}_k \quad k = 1, \ldots, K, \end{array} \right. \\ H_1 & : & \left\{ \begin{array}{ll} \mathbf{y} & = \mathbf{s} + \mathbf{c} + \mathbf{n} \\ \mathbf{y}_k & = \mathbf{c}_k + \mathbf{n}_k \quad k = 1, \ldots, K, \end{array} \right. \end{array} \tag{3}$$

where $\mathbf{s}$ is the useful signal associated with the target, $\mathbf{c}$ is the clutter contribution, $\mathbf{n}$ the noise contribution for the primary data, H_0 and H_1 are the null and target-present hypotheses respectively; we use the same notation for the secondary data. We now develop the signal and the interference models in some detail.

2.1 Signal model

This section focuses on the target contribution to the received signals. The signal transmitted by the n^{th} element of the array is

$$x_n(t) = u_n(t) e^{j2\pi f_0 t + j\psi}, \tag{4}$$

where ψ is a random phase, $j = \sqrt{-1}$ and $u_n(t)$ is the complex envelope of the FM pulse given by

$$u_n(t) = \sum_{m=0}^{M-1} u_{pn}(t - mT_r), \tag{5}$$

where $u_{pn}(t)$ is the envelope of the single pulse. The transmitted signal is reflected by the target and it is received by all the sub-apertures. The signal received at the i^{th} receiver is

$$r_{in}(t) = \alpha_t u_n(t - \tau_{Lin}) e^{j2\pi(f_0 + f_{dn})(t - \tau_{Lin})}, \tag{6}$$

where α_t is the amplitude (the phase ψ is also included), f_{dn} is the Doppler frequency relative to the n^{th} transmission and τ_{Lin} is the total trip delay, due to the delay from the n^{th} transmitter to the look point (X_L, Y_L, Z_L) plus the delay from the target to the i^{th}

receiver

$$\tau_{Lin} = \frac{\sqrt{(x_n - X_L)^2 + (y_n - Y_L)^2 + Z_L^2} + \sqrt{(x_i - X_L)^2 + (y_i - Y_L)^2 + Z_L^2}}{c}. \quad (7)$$

The received signal (6) is delayed by the amount ΔT_i, so that the same range gate is used at all elements. After this delay and downconversion, the signal becomes

$$\tilde{r}_{in}(t) = \alpha_t u_n(t - \tau_{Lin} - \Delta T_i) e^{-j2\pi f_0 \tau_{Lin}} e^{j2\pi f_{dn}(t - \tau_{Lin} - \Delta T_i)}. \quad (8)$$

Applying the matched filter the signal becomes

$$\begin{aligned} s_{in}(t) &= \int_{-\infty}^{+\infty} \tilde{r}_{in}(\tau) u_{pn}^*(\tau - t) d\tau, \\ &= \int_{-\infty}^{+\infty} \alpha_t u_n(\tau - \tau_{Lin} - \Delta T_i) e^{-j2\pi f_0 \tau_{Lin}} e^{j2\pi f_{dn}(\tau - \tau_{Lin} - \Delta T_i)} u_{pn}^*(\tau - t) d\tau, \\ &= \alpha_t e^{-j2\pi f_0 \tau_{Lin}} \int_{-\infty}^{+\infty} e^{j2\pi f_{dn}(\tau - \tau_{Lin} - \Delta T_i)} \sum_{m=0}^{M-1} u_{pn}(\tau - \tau_t) u_{pn}^*(\tau - t) d\tau, \end{aligned} \quad (9)$$

$$\begin{aligned} &= \alpha_t e^{-j2\pi f_0 \tau_{Lin}} \sum_{m=0}^{M-1} e^{j2\pi f_{dn} m T_r} \int_{-\infty}^{+\infty} u_{pn}(\beta) u_{pn}^*[\beta - (t - \tau_t)] e^{j2\pi f_{dn} \beta} d\beta, \\ &= \alpha_t e^{-j2\pi f_0 \tau_{Lin}} \sum_{m=0}^{M-1} e^{j2\pi f_{dn} m T_r} \chi_n(t - \tau_t, f_{dn}), \end{aligned} \quad (10)$$

where $\tau_t = mT_r + \tau_{Lin} + \Delta T_i$ and $\chi_n(\tau, f)$ is the ambiguity function relative to the n^{th} transmission evaluated for the delay $t - mT_r - \tau_{Lin} - \Delta T_i$. Note that the total delay $\tau_{Lin} + \Delta T_i$ is constant with respect to index i and is equal to

$$\begin{aligned} \tau_{Lin} + \Delta T_i &= \frac{D_i}{c} + \frac{D_n}{c} + \frac{\max_p\{D_p\}}{c} - \frac{D_i}{c}, \\ &= \frac{\max_p\{D_p\} + D_n}{c}. \end{aligned} \quad (11)$$

The signal in (10) is sampled at $t = t_s = mT_r + \tau_{Lin} + \Delta T_i$ resulting in

$$\begin{aligned} s_{inm}(t_s) &= \alpha_t e^{-j2\pi f_0 \tau_{Lin}} e^{j2\pi f_{dn} m T_r} \chi_n(t_s - \tau_c, f_{dn}), \\ &= \alpha_t e^{-j2\pi f_0 \tau_{Lin}} e^{j2\pi f_{dn} m T_r} \chi_n(0, f_{dn}). \end{aligned} \quad (12)$$

This sample represents the target contribution to the i^{th} receive element due to the transmission from the n^{th} antenna at the m^{th} pulse in the CPI.

The $NM \times 1$ steering vector relative to the n^{th} transmission is composed by all the samples over the indices i and m

$$\mathbf{s}_n = \begin{bmatrix} s_{0n0} \\ \vdots \\ s_{(N-1)n0} \\ s_{0n1} \\ \vdots \\ s_{(N-1)n1} \\ s_{0n2} \\ \vdots \\ s_{(N-1)n(M-1)} \end{bmatrix}. \tag{13}$$

We introduce the temporal steering vector $\mathbf{b}_n(\varpi_n)$ and the spatial steering vector $\mathbf{a}_n(\vartheta_n)$ defined as

$$\mathbf{b}_n(\varpi_n) = \left[1,\, e^{j2\pi\varpi_n},\, e^{j2\pi 2\varpi_n}, \ldots, e^{j2\pi(M-1)\varpi_n}\right]^T, \tag{14}$$

$$\mathbf{a}_n(\vartheta_n) = \chi_n(0, f_{dn}) \left[e^{-j2\pi f_0 \tau_{L0n}}, \ldots, e^{-j2\pi f_0 \tau_{L(N-1)n}}\right]^T, \tag{15}$$

where $(\cdot)^T$ denotes the transpose operator and

$$\varpi_n = f_{dn} T_r = f_{dn}/f_r, \tag{16}$$

is the normalized Doppler frequency relative to the n^{th} transmission and

$$\vartheta_n = \left[f_0 \tau_{L0n}, \ldots, f_0 \tau_{L(N-1)n}\right]^T, \tag{17}$$

is the vector of the spatial frequencies relative to the n^{th} transmission. Finally, we can express the target steering vector as

$$\mathbf{s}_n = \alpha_t \mathbf{b}_n(\varpi_n) \otimes \mathbf{a}_n(\vartheta_n), \tag{18}$$

where $\otimes$ denotes the Kronecker product of two matrices.

2.2 Interference model

The interference is due to two statistically independent components, thermal noise and clutter modeled as a chaff cloud. As in [10], we model the clutter as the sum of many low power discretes; here they form a ball surrounding the target. Let us assume N_c as the number of discrete clutter sources. We assume that the noise components $\mathbf{n}$ and

$\mathbf{n}_k\,, k = 1, \ldots, K$ are independent complex circular Gaussian vectors with zero mean and covariance matrix given by

$$\mathbf{R}_{no} = E\{\mathbf{n}\mathbf{n}^H\} = E\{\mathbf{n}_k\mathbf{n}_k^H\} = \sigma^2\mathbf{I}, \tag{19}$$

where $\mathbf{I}$ denotes an identity matrix of required order, $E\{\cdot\}$ denotes statistical expectation and $(\cdot)^H$ the Hermitian or conjugate transpose.

An artifact (i.e., a clutter discrete) at $\left(x^l, y^l, z^l\right)$ reflects the incoming wave given by (4). The received signal at the i^{th} element due to the n^{th} transmission reflected by the l^{th} artifact is

$$r_{inl}(t) = A_{nl}u_n(t - \tau_{inl})e^{j2\pi(f_0+f_{dnl})(t-\tau_{inl})}, \tag{20}$$

where A_{nl} is a random amplitude that includes also the random phase, f_{dnl} is the Doppler frequency relative to the l^{th} artifact and the n^{th} transmission and τ_{inl} is the total delay from the n^{th} transmitter to the l^{th} artifact plus the delay from the artifact to the i^{th} receiver

$$\tau_{inl} = \frac{\sqrt{(x_n - x^l)^2 + (y_n - y^l)^2 + (z^l)^2} + \sqrt{(x_i - x^l)^2 + (y_i - y^l)^2 + (z^l)^2}}{c}. \tag{21}$$

The artifact is not located at the look point. Note that, if required, the return due to a target not at the look point can be included as a discrete clutter source. Figure 2 illustrates the total trip delay involving the look-point and the one involving the artifact.

The received signal due to the artifact is treated in the same manner as the signal due to the target. Using the same development as in the previous subsection, we can write the final signal due to the artifact, after delaying, down conversion and matched filtering, as

$$c_{inl}(t) = A_{nl}e^{-j2\pi f_0\tau_{inl}} \sum_{m=0}^{M-1} e^{j2\pi f_{dnl}mT_r}\chi_n(t - mT_r - \tau_{inl} - \Delta T_i, f_{dnl}), \tag{22}$$

similar to (10); note that the only differences are in the total trip delay where τ_{inl} is used instead of τ_{Lin}, in the Doppler frequency (f_{dnl} instead of f_{dn}) and in the amplitude (A_{nl} instead of α_t). A generic element at the i^{th} receiver, due to the n^{th} transmission and to l^{th} artifact and at the m^{th} pulse can be written as

$$c_{inml}(t) = A_{nl}e^{-j2\pi f_0\tau_{inl}}e^{j2\pi f_{dnl}mT_r}\chi_n(t - mT_r - \tau_{inl} - \Delta T_i, f_{dnl}). \tag{23}$$

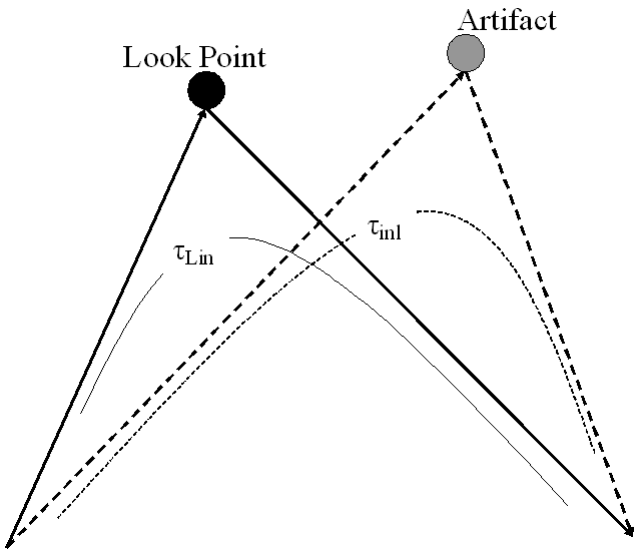

Figure 2: *Total trip delays involving the target (solid line) and the artifact (dashed line).*

The next section deals with the use of space-time adaptive processing to detect the target buried in relatively strong interference. To do so, we need to estimate the unknown interference covariance matrix. As is common in STAP, we estimate this matrix from the environment using the secondary data. Estimating the covariance matrix involves sampling c_{inml} at the range gates straddling the look point's range gate. The time of the samples is given by

$$t_k = mT_r + \tau_{Lin} + \Delta T_i + kT_s, \tag{24}$$

where T_s is the additional delay due to the k-th secondary range cell and the integer $k \in [-\lceil K/2 \rceil, \lfloor K/2 \rfloor]$, where $\lceil \cdot \rceil$ denotes the rounding off to the higher integer and $\lfloor \cdot \rfloor$ denotes the rounding off to the lower integer. Sampling the received signal in (22) every t_k yields

$$\hat{c}_{inmlk} = A_{nl} e^{-j2\pi f_0 \tau_{inl}} e^{j2\pi f_{dnl} m T_r} \chi_n(\tau_{Lin} - \tau_{inl} + kT_s, f_{dnl}). \tag{25}$$

Summing over all the N_c unambiguous interference sources we can write the sample relative to the n^{th} transmission, the i^{th} receiver, the m^{th} pulse and the k^{th} secondary range gate as

$$\hat{c}_{inmk} = \sum_{l=0}^{N_c-1} A_{nl} e^{-j2\pi f_0 \tau_{inl}} e^{j2\pi f_{dnl} m T_r} \chi_n(\tau_{Lin} - \tau_{inl} + kT_s, f_{dnl}). \tag{26}$$

As with the target signal in the previous section, we assemble these samples to obtain the length-NM steering vector of the clutter source $\mathbf{c}_{nk}$ relative to the n^{th} transmission and

the k^{th} range cell

$$\mathbf{c}_{nk} = \begin{bmatrix} c_{0n0k} \\ \vdots \\ c_{(N-1)n0k} \\ c_{0n1k} \\ \vdots \\ c_{(N-1)n1k} \\ c_{0n2k} \\ \vdots \\ c_{(N-1)n(M-1)k} \end{bmatrix}. \tag{27}$$

Figure 3 shows the geometry of the isorange contours for a bistatic configuration; they are ellipses wich foci are the transmitter and the receiver.

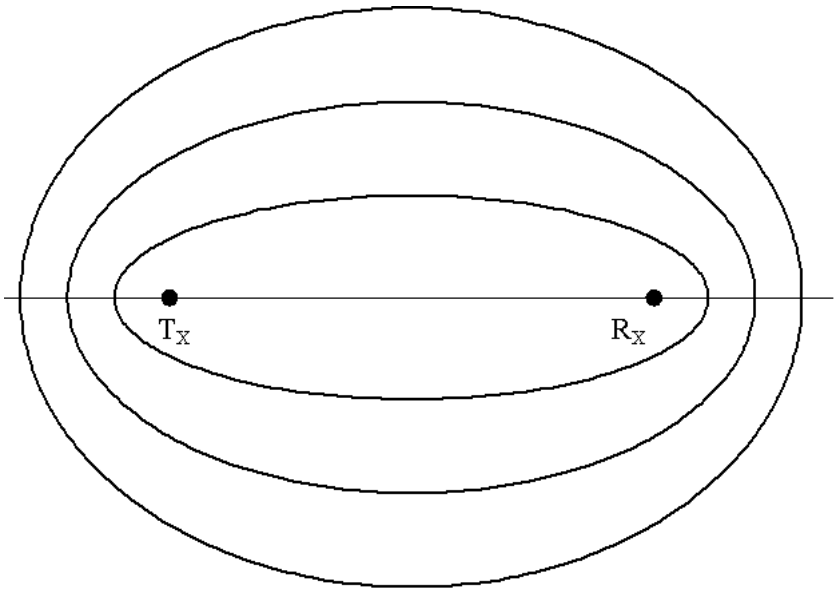

Figure 3: Isorange contours for a bistatic configuration.

2.3 STAP implementation

We can now implement STAP using the modified sample matrix inversion (MSMI) [19] statistic for target detection. As usual, we estimate the interference covariance matrix from secondary data. Due to the time-orthogonality of the N transmitted waveforms, the interference covariance matrix is block-diagonal

$$\hat{\mathbf{R}} = \begin{bmatrix} \hat{\mathbf{R}}_0 & 0 & \dots & 0 \\ 0 & \hat{\mathbf{R}}_1 & \dots & 0 \\ \vdots & \vdots & \ddots & \vdots \\ 0 & 0 & \dots & \hat{\mathbf{R}}_{(N-1)} \end{bmatrix}, \tag{28}$$

where

$$\hat{\mathbf{R}}_n = \frac{1}{K} \sum_{k=-\lceil K/2 \rceil}^{\lfloor K/2 \rfloor} \mathbf{y}_{nk} \mathbf{y}_{nk}^H,$$

is the n^{th} block of the matrix in (28) and is relative to the n^{th} transmission. The vectors $\mathbf{y}_{nk}$ are the secondary data collected from the environment for the n^{th} transmission; they include the additive Gaussian noise and clutter. Due to the independence of noise and clutter contributions, the matrix is

$$\hat{\mathbf{R}}_n = \hat{\mathbf{R}}_{no} + \hat{\mathbf{R}}_{cn}, \tag{29}$$

where $\hat{\mathbf{R}}_{cn}$ is the $(NM) \times (NM)$ clutter covariance matrix relative to the n^{th} transmission. Note that the noise contribution is independent of the transmission index. Using the matrices defined in (28) and recalling that the inverse of a block diagonal matrix is a block diagonal matrix which blocks are the inverse of the corresponding blocks in the initial matrix, we can calculate the weight vectors for each bistatic problem

$$\mathbf{w}_n = \hat{\mathbf{R}}_n^{-1} \mathbf{s}_n, \tag{30}$$

where $\mathbf{s}_n$ is length-NM space-time steering vector from (13) corresponding to the look point. The overall length-N^2M steering vector is given by

$$\mathbf{s} = \begin{bmatrix} \mathbf{s}_0 \\ \mathbf{s}_1 \\ \vdots \\ \mathbf{s}_{(N-1)} \end{bmatrix}. \tag{31}$$

Finally, the *coherent* output MSMI statistic is [19]

$$\text{MSMI} = \frac{\left| \sum_{n=0}^{N-1} \mathbf{w}_n^H \mathbf{y}_n \right|^2}{\left| \sum_{n=0}^{N-1} \mathbf{w}_n^H \mathbf{s}_n \right|}. \tag{32}$$

where $\mathbf{y}_n$ is the received signal for the n^{th} transmission. Note that the statistic assumes coherence across all the transmissions. This is possible because, unlike the frequency diversity case of [2], all transmissions share a common center frequency. Implementation difficulties to maintain this phase coherence is outside the scope of this paper. Note that the computational complexity of the MSMI statistic is $O(N^2M)$.

3 Clutter non-stationarity

One of the advantages of the orthogonal signaling is that each transmission can be treated independently at each receiver. The orthogonality implies that the initial multistatic problem is essentially a superposition of a series of individual bistatic problems and we can use results from the bistatic theory for our treatment. In particular, the non-stationary nature of ground-based clutter in bistatic airborne radar is well known [14]; in this configuration the motion of either transmitter and receiver causes the range dependency of the clutter. In our system the motion is due to the artifact, while both transmitter and receiver are ground-based and we have to reconsider the bistatic problem in the context of the waveform diversity. As demonstrated in [2] this non-stationarity affects the output of the STAP processor.

The basic hypothesis of the space-time adaptive processing is the stationarity of the environment. In fact, the secondary data are collected from range gates close to the one under test and are used to estimate the covariance matrix of the interference; the quality of this estimation depends on the stationarity of the environment. Due to the range dependency of the clutter Doppler frequency, this hypothesis is no longer valid. It is therefore important to study this phenomenon in the context of waveform diversity. Figure 4 shows the geometry of the system, where Ar is the artifact, $\mathbf{v}$ is its velocity, θ_T, θ_R and θ_v are, respectively, the elevation angles of the transmitter-artifact path, of the receiver-artifact path and of the artifact velocity, φ_T, φ_R and φ_v are, respectively, the azimuth angles of the transmitter-artifact path, of the receiver-artifact path and of the artifact velocity. Note that each clutter source of the ball has the same velocity vector $\mathbf{v}$. The direction of the interference sources is fixed and determined by the angles θ_v and φ_v.

The clutter Doppler frequency due to the motion is

$$f_D = f_{Dx} + f_{Dy} + f_{Dz}, \tag{33}$$

where

$$f_{Dx} = \frac{\mathbf{v}\cos\theta_v\cos\varphi_v[\cos\theta_T\cos\varphi_T + \cos\theta_R\cos\varphi_R]}{\lambda}, \tag{34}$$

$$f_{Dy} = \frac{\mathbf{v}\cos\theta_v\sin\varphi_v[\cos\theta_T\sin\varphi_T + \cos\theta_R\sin\varphi_R]}{\lambda}, \tag{35}$$

$$f_{Dz} = \frac{\mathbf{v}\sin\theta_v[\sin\theta_T + \sin\varphi_R]}{\lambda}. \tag{36}$$

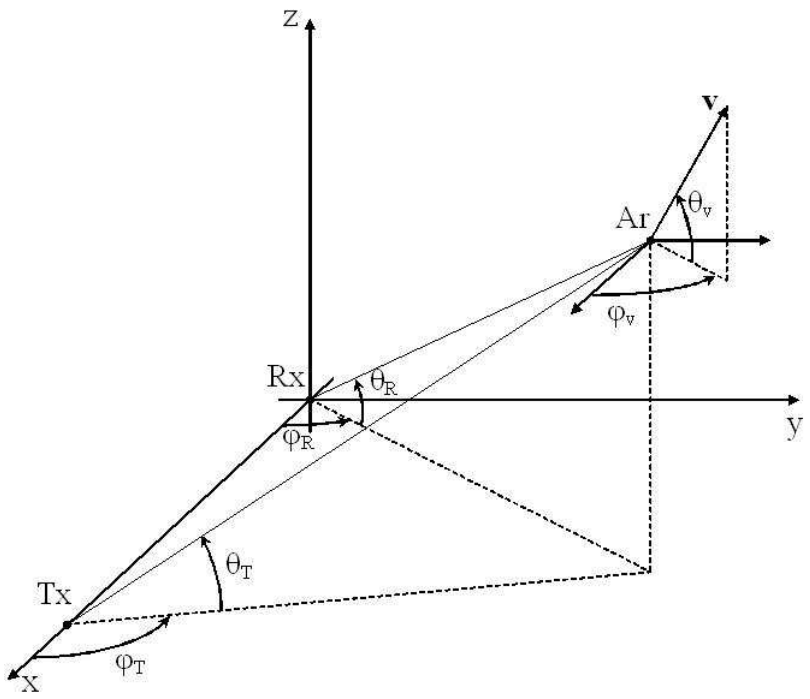

Figure 4: *Geometry of bistatic ground radar.*

The threesome of transmitter/receiver/scatterer Ar identifies the bistatic plane; so, there is a different plane for each transmitter/receiver pair. It is defined by the axes $x-y_b$ and is characterized by the elevation angle θ_b with respect to the reference (x, y). The iso-range contour, which lies in this plane, is shown in the Figure 5; it is an ellipse with foci at the transmitter and the receiver with major axis a and minor axis $b = \sqrt{a^2 - L^2/4}$, where L is the distance between the transmitter and the receiver. We can use the points of this ellipse to evaluate the Doppler frequency of the scatterer along the iso-range contour; each evaluation point along the ellipse is characterized by the azimuth angle φ_e, used to take a spatial sample along the iso-range contour. This choice makes comparable the plots concerning different ellipses. To evaluate the range dependency we need to change the contour. A new ellipse is defined changing the major axis; the new axis is defined as

$$a' = a + (c\tau_p)/2, \tag{37}$$

where c is the light speed and τ_p is the pulse width; the new minor axis is $b' = \sqrt{a'^2 - L^2/4}$. Figure 6 plots the Doppler frequency of the clutter using (33) for different range cells in function of the azimuth angle in the bistatic plane. The non-stationarity of the clutter Doppler frequency is readily apparent.

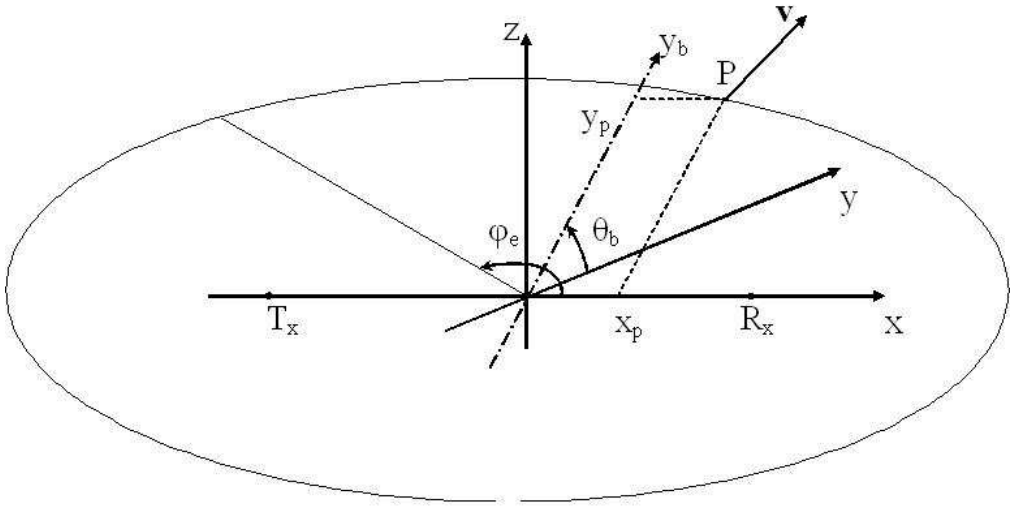

Figure 5: *Bistatic plane with bistatic ellipse. The axes origin is in the middlepoint of the baseline, i.e. the line where transmitter and receiver lie.*

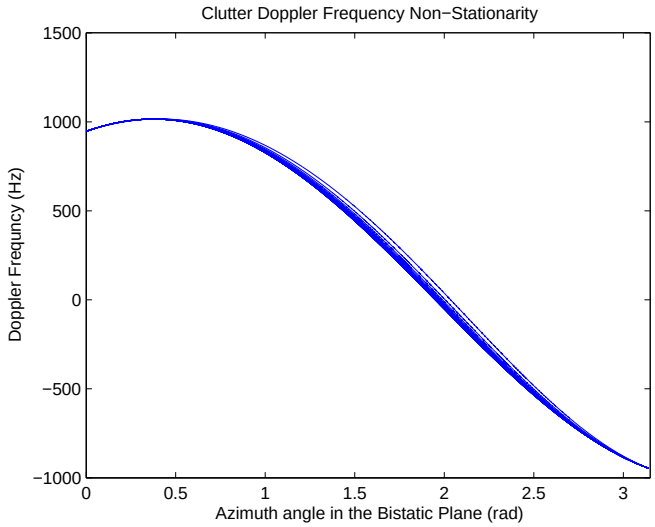

Figure 6: *Clutter Doppler frequency plotted for different range cells.*

3.1 JDL algorithm for distributed aperture radars

To improve the performance of the STAP algorithm over that given in [2] we account for the clutter non-stationarity by modifying the STAP processing [14]. Essentially, clutter non-stationarity limits the number of statistically homogeneous secondary data samples available. The Reed-Mallet-Brennan (RMB) rule suggests that one needs twice the number of secondary samples as the number of degrees of freedom [20], i.e., using all possible degrees of freedom is likely impossible. Motivated by this issue, we use the reduced dimension Joint Domain Localized (JDL) algorithm. The JDL algorithm adaptive processes the data after transformation from the space-time to the angle-Doppler domain. This algorithm has been shown to perform well in non-stationary environments [16, 21, 22]. The work in [21, 22] was the first which studied the need of the limited training-data size of the localized adaptive processing in non-homogeneous and non-stationary environments; it was shown that JDL outperforms fully adaptive processing using all adaptive degrees of freedom, in these scenarios.

The JDL algorithm reduces the number of degrees of freedom by processing only the data within a localized processing region (LPR). The LPR, comprising η_a angles and η_d Doppler bins, is centered around the look angle-Doppler. The number of adaptive unknowns is therefore reduced from NM in the space-time domain to $\eta_a\eta_d$ in the angle-Doppler domain per transmission. Figure 7 presents a pictorial view of the processing scheme, where the bin marked as "Signal" indicates the target location in angle-Doppler domain.

The original formulation of the JDL algorithm uses a two dimensional DFT to convert the data from the space-time domain to the angle-Doppler one. This formulation is possible assuming that the receiving antenna is an equi-spaced linear array of isotropic, ideal, point sensors. When applying the JDL algorithm to real systems, this crucial assumption is no longer valid; the elements of a real array cannot be point sensors. Furthermore, the assumption of linear equi-spaced array is restrictive. In any case, both these assumptions are invalid in our case of distributed aperture radars. We therefore need to resort to a more general formulation [23].

The formulation in [23] replaces the DFT with a transformation matrix, $\mathbf{T}$, that comprises the steering vectors associated with the η_a angles and η_d Doppler bins. This approach is based on the fact that estimating the response at a specific angle-Doppler

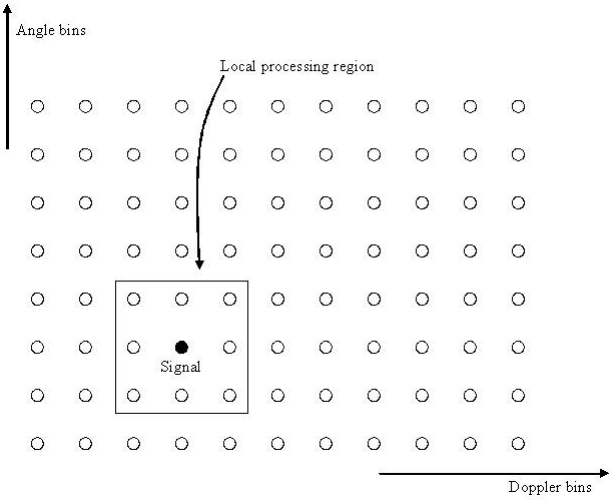

Figure 7: *Localised processing region in angle-Doppler domain for $\eta_a = \eta_d$=3.*

point requires an inner product with the corresponding steering vector. Note that since each transmission uses a different time delay, the transformation matrix is different for each of the N transmissions. The transformation matrix for the n^{th} transmission is defined as

$$\mathbf{T}_n = \mathbf{b}_n(\mathbf{\Omega}_n) \otimes \mathbf{a}_n(\mathbf{\Theta}_n), \tag{38}$$

where the vector $\mathbf{\Omega}_n$ is the vector of Doppler frequencies normalized by the PRF, centered at the Doppler of the target and spaced by $1/M$ and $\mathbf{\Theta}_n$ is the vector of the spatial frequencies for the different angles of arrivals; in this paper we use an angle spacing in azimuth equal to $\Delta(\varphi) = \pi/N$.

We need to evaluate the relative propagation delays from point defined by each angle. Each element of the length-N vector $\mathbf{\Theta}_n$ has to be evaluated considering the round trip delay from the n^{th} transmitter to the i^{th} receiver through the new look point while changing only the azimuth angle by the amount π/N. The point is located in the space by the same elevation angle θ_T of the target and the same distance from the origin of coordinates system to the target. The transformation matrix is defined as

$$\mathbf{T}_n = \left[\mathbf{b}_n(\varpi_{n(-ai)}), \ldots, \mathbf{b}_n(\varpi_{n(0)}), \ldots, \mathbf{b}_n(\varpi_{n(ai)})\right] \otimes \left[\mathbf{a}_n(\vartheta_{n(-Di)}), \ldots, \mathbf{a}_n(\vartheta_{n(0)}), \ldots, \mathbf{a}_n(\vartheta_{n(Di)})\right], \tag{39}$$

where

$$ai = \left\lceil \frac{\eta_a}{2} \right\rceil \quad Di = \left\lceil \frac{\eta_d}{2} \right\rceil, \tag{40}$$

and

$$\varpi_{n(h)} = \frac{f_{dn}}{f_r} + \frac{h}{M}, \quad \vartheta_{n(h)} = \left[f_0\tau_{L0n(h)}, \ldots, f_0\tau_{L(N-1)n(h)}\right]^T, \tag{41}$$

where $\tau_{Lin(h)}$ is the delay associated with the path from the n^{th} transmitter to the i^{th} receiver through the point which the azimuth angle is $\varphi_t + (h\pi)/N$ and the elevation angle is the same as that of the target. For example, if η_a=3 and η_d=3 this matrix is

$$\mathbf{T}_n = \left[\mathbf{b}_n(\varpi_{n(-1)}), \mathbf{b}_n(\varpi_{n(0)}), \mathbf{b}_n(\varpi_{n(1)})\right] \otimes \left[\mathbf{a}_n(\vartheta_{n(-1)}), \mathbf{a}_n(\vartheta_{n(0)}), \mathbf{a}_n(\vartheta_{n(1)})\right], \tag{42}$$

where

$$\begin{aligned}
\varpi_{n(-1)} &= \frac{f_{dn}}{f_r} - \frac{1}{M}, \\
\varpi_{n(1)} &= \frac{f_{dn}}{f_r} + \frac{1}{M}, \\
\vartheta_{n(-1)} &= \left[f_0\tau_{L0n(-1)}, \ldots, f_0\tau_{L(N-1)n(-1)}\right]^T, \\
\vartheta_{n(+1)} &= \left[f_0\tau_{L0n(+1)}, \ldots, f_0\tau_{L(N-1)n(+1)}\right]^T.
\end{aligned}$$

We can now define the vectors in the angle-Doppler domain using the matrix $\mathbf{T}_n$ defined above. The relevant transformation is a multiplication with the $(\eta_a\eta_d \times NM)$ transformation matrix $\mathbf{T}_n$. The transformation matrix multiplies the primary and secondary data and the steering vector associated with the look point. The transformed steering vector and the received signal for the n^{th} transmission in the angle-Doppler domain are respectively

$$\mathbf{s}_{naD} = \mathbf{T}_n^H \mathbf{s}_n, \tag{43}$$

$$\mathbf{y}_{naD} = \mathbf{T}_n^H \mathbf{y}_n, \tag{44}$$

where the subscript aD denotes the vector in the angle-Doppler domain. At the same way we can convert the secondary data in the angle-Doppler domain

$$\mathbf{y}_{nkaD} = \mathbf{T}_n^H \mathbf{y}_{nk}, \tag{45}$$

needed to evaluate the covariance matrix of the interference in the angle-Doppler domain

$$\hat{\mathbf{R}}_{naD} = \frac{1}{K} \sum_{k=K_i}^{K_s} \mathbf{y}_{nkaD} \mathbf{y}_{nkaD}^H, \tag{46}$$

where

$$K_i = \left\lfloor \frac{K}{2} \right\rfloor \qquad K_s = \left\lceil \frac{K}{2} \right\rceil$$

and the weight vector

$$\mathbf{w}_{naD} = \hat{\mathbf{R}}_{naD}^{-1}\mathbf{s}_{naD}. \tag{47}$$

We can now evaluate the decision statistic in the angle-Doppler domain as in (32) for the space-time domain

$$\mathrm{MSMI}_{aD} = \frac{\left|\sum_{n=0}^{N-1} \mathbf{w}_{naD}^{H}\mathbf{y}_{naD}\right|^2}{\left|\sum_{n=0}^{N-1} \mathbf{w}_{naD}^{H}\mathbf{s}_{naD}\right|}. \tag{48}$$

Note that the computational complexity of the MSMI_{aD} statistic is $O(N^2 M \eta_a^2 \eta_d^2)$.

4 CFAR behavior

We now show that the MSMI test statistic developed in Section 2 is independent of the true interference covariance matrix under hypotheses H_0 and this gives it a constant false alarm rate.

The interference is composed by two contributions, clutter and noise. As reported previously, the noise is Gaussian colored noise with zero mean and covariance matrix $\mathbf{R}_{no}$ and this holds for each transmission. The clutter therm is characterized by a Gaussian distribution with zero mean and covariance matrix $\mathbf{R}_{cn}$ for each transmission [24]. The two contributions are uncorrelated, as reported in (29), for each transmission. We can conclude that the interference contribution $\mathbf{h}_n = \mathbf{c}_n + \mathbf{n}_n$ is a Gaussian random vector with zero mean and covariance matrix $\mathbf{R}_n$. Let now be $\mathbf{z}_n = \mathbf{R}_n^{-1/2}\mathbf{y}_n$ the whitened data vector and $\mathbf{r}_n = \mathbf{R}_n^{-1/2}\mathbf{s}_n$ the "whitened" steering vector; the test statistic (32) can be written as

$$\frac{\left|\sum_{n=0}^{N-1} \mathbf{r}_n^{\dagger}\mathbf{R}_n^{1/2}\hat{\mathbf{R}}_n^{-1}\mathbf{R}_n^{1/2}\mathbf{z}_n\right|^2}{\left|\sum_{n=0}^{N-1} \mathbf{r}_n^{\dagger}\mathbf{R}_n^{1/2}\hat{\mathbf{R}}_n^{-1}\mathbf{R}_n^{1/2}\mathbf{r}_n\right|} = \frac{\left|\sum_{n=0}^{N-1} \mathbf{r}_n^{\dagger}\tilde{\mathbf{R}}_n^{-1}\mathbf{z}_n\right|^2}{\left|\sum_{n=0}^{N-1} \mathbf{r}_n^{\dagger}\tilde{\mathbf{R}}_n^{-1}\mathbf{r}_n\right|}, \tag{49}$$

where the matrix $\tilde{\mathbf{R}}_n = \mathbf{R}_n^{-1/2}\hat{\mathbf{R}}_n\mathbf{R}_n^{-1/2}$ is subject to the complex Wishart distribution with parameter K, NM and $\mathbf{I}$, which is denoted as $CW(K, NM; \mathbf{I})$ [25].

Now we define a unitary transform that rotates the whitened signal vector into the first elementary vector

$$b\mathbf{e}_n = \mathbf{U}_n^{\dagger}\mathbf{r}_n,\ \mathbf{e}_n = [1, 0, \ldots, 0]^{\dagger}. \tag{50}$$

The first column of $\mathbf{U}_n$ is the vector $\mathbf{r}_n$ and the others $(NM-1)$ ones form an arbitrary orthonormal basis of the orthogonal complement of the subspace spanned by the vector

$\mathbf{r}_n$. Then the test (49) becomes

$$\frac{\left|\sum_{n=0}^{N-1} b\mathbf{e}_n^\dagger \mathbf{U}_n^\dagger \tilde{\mathbf{R}}_n^{-1} \mathbf{U}_n \mathbf{g}_n\right|^2}{\left|\sum_{n=0}^{N-1} b^2 \mathbf{e}_n^\dagger \mathbf{U}_n^\dagger \tilde{\mathbf{R}}_n^{-1} \mathbf{U}_n \mathbf{e}_n\right|} = \frac{\left|\sum_{n=0}^{N-1} b\mathbf{e}_n^\dagger \mathbf{B}_n^{-1} \mathbf{g}_n\right|^2}{\left|\sum_{n=0}^{N-1} b^2 \mathbf{e}_n^\dagger \mathbf{B}_n^{-1} \mathbf{e}_n\right|} \tag{51}$$

where $\mathbf{g}_n = \mathbf{U}_n^\dagger \mathbf{z}_n$ and $\mathbf{B}_n = \mathbf{U}_n^\dagger \tilde{\mathbf{R}}_n \mathbf{U}_n$. The vector $\mathbf{g}_n$ is Gaussian distributed with zero mean and covariance matrix $\mathbf{I}$ under H_0 hypotheses and the matrix $\mathbf{B}_n$ is distributed $CW(K, NM; \mathbf{I})$.

The actual covariance matrix does not appear in the test statistic or in the underlying density functions; the test statistic is independent of both the structure and the level of the true covariance matrix and is, therefore, a CFAR test.

We can repeat the analysis made above for the test statistic defined in (32) for the one defined in (48) applying the JDL algorithm to the classic MSMI. The only difference is that the vectors are now defined by a linear transformation of the initial vectors, as in (43)-(45). This transformation does not change the statistical distribution of the vectors; therefore we can repeat the previous analysis substituting the vectors $\mathbf{y}_n$ and $\mathbf{s}_n$ and the matrix $\hat{\mathbf{R}}_n$ respectively with $\mathbf{y}_{naD}$, $\mathbf{s}_{naD}$ and $\hat{\mathbf{R}}_{naD}$. So the CFAR behavior holds also for this test statistic as well.

5 Numerical simulations

In this section we present the results of numerical simulations using the models developed in Sections 2 and 3. Results reported in [2] had demonstrated the importance of the use of waveform diversity for distributed aperture radars in order to deal with the problem of the grating lobes. Since the steering vectors are range dependent, the beam-pattern is a plot of the signal strength versus the transverse, x, coordinate. The range dependency implies a small decay in the level of the grating lobes further away from the target location. However, this decay is inadequate for target detection. Using frequency diversity proposed in [2] it is possible to eliminate the grating lobes. We expect that using time-based diversity the grating lobes are worse than that achievable with frequency diversity, i.e., the benefits of coherent processing arise at the cost of high grating lobes. We expect also that the application of the JDL algorithm, which takes into account the non-stationarity of the environment, improves the achievable performance in terms of an improved detection probability.

Parameter	Value	Parameter	Value
N	9	M	3
T_{MIN}	$10\mu s$	T_{MAX}	$100\mu s$
B	10MHz	f_0	10GHz
PRI	T_r	INR	50dB
Target Velocity	50m/s	Target SNR	10dB
X_t	476.9158m	Y_t	-59.9566m
Z_t	200km	N_c	200

Table 1: Parameters common to the simulations.

The experiments use the common parameters shown in the Table 1. In the table T_{MIN} and T_{MAX} represent the minimum and the maximum pulse duration respectively; the pulse repetition time (PRI) is

$$T_r = 5 \sum_{n=0}^{N-1} T(n), \tag{52}$$

where $T(n)$ is the n^{th} pulse duration equal to

$$T(n) = T_{MIN} + n \frac{T_{MAX} - T_{MIN}}{N-1}. \tag{53}$$

The array elements are uniformly distributed in the (x, y) plane on a square $200m \times 200m$ grid. INR is the Interference-to-Noise Ratio.

5.1 Need for waveform diversity

In this subsection we report using waveform diversity in the original space-time domain using the decision statistic in (32). These first results allow us to analyze the impact of the proposed waveform diversity scheme on the system performance independent of the improvement achievable with the JDL algorithm. In this way it is possible to understand how the proposed model counters the central issue of grating lobes in a distributed radar system.

Figure 8 plots the output of the matched filter along the radial z-direction. The target is at a range of 200km in the radial z-direction. The output is very asymmetric due to the range dependency of the clutter that affects the estimation of the covariance matrix. Figure 9 plots similar results along the transverse x-direction. The high grating lobes are clear, i.e, the benefits of coherent processing are possible at the cost of grating lobes. The target is at a range of 476.9158m in the transverse x-direction. The output of the matched filter is more regular and symmetric than the one in the radial direction.

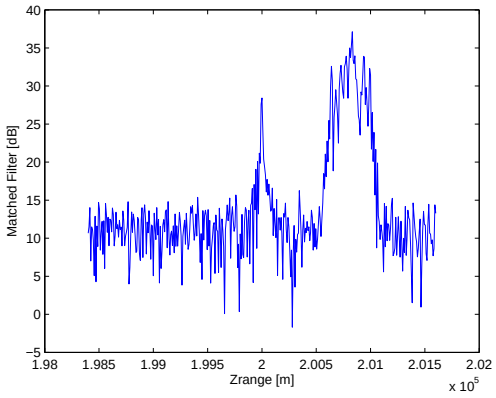

Figure 8: Matched filter processing along the radial Z-direction. Includes interference.

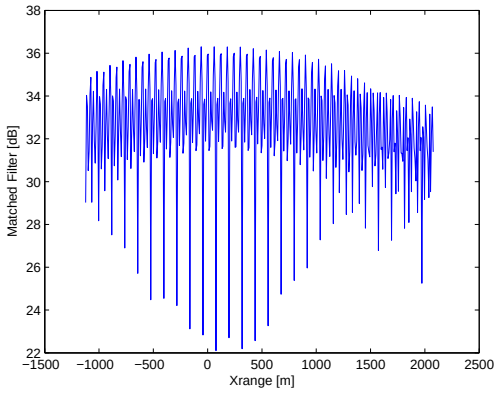

Figure 9: Matched filter processing along the transverse X-direction. Includes interference.

Figure 10 plots the modified sample matrix inversion (MSMI) statistic over the radial z-direction. All interference range cells are used to estimate the interference covariance matrix. The target is very clearly identified, even using only 3 pulses and 9 antenna elements, due to the narrow lobe centered at 200km in range, that is, at the target range. Figure 11 plots similar results along the transverse x-direction. In this case the target in not clear identifiable and the system shows a performance decay. This is again because of the grating lobes.

These plots show that the waveform diversity model used allows for good target detection in the radial z-direction. However, these results, coupled with the work in [2] underline an essential issue with using distributed apertures - the work in [2] used frequency diversity to eliminate grating lobes. However frequency diversity requires coherent processing over an extremely wide frequency band. In this work we have investigated time diversity using varying FM rates raising the issue of grating lobes in the transverse, x,

direction. The benefits of both may be achievable using orthogonal frequency division multiplexing (OFDM) [26].

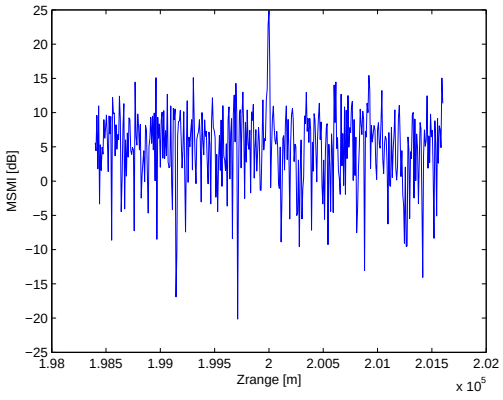

Figure 10: MSMI statistic along the radial Z-direction. Includes interference.

5.2 Performance of the JDL algorithm

In this subsection we illustrate the performance improvements achievable using the JDL processing algorithm. For this purpose we compare between the decision statistic obtained using the waveform diversity in (32) and the one obtained when coupling waveform diversity with the JDL algorithm (as in (48)). In this way it is possible to study the benefits of using reduced dimension schemes. At the same time we also compare these performances with that ones achievable using the frequency diversity model in [3] to analyze the achievable improvements with respect to this approach. In the following, we indicate the decision statistic in [3] as **F-MSMI** (Frequency MSMI), the one obtained using

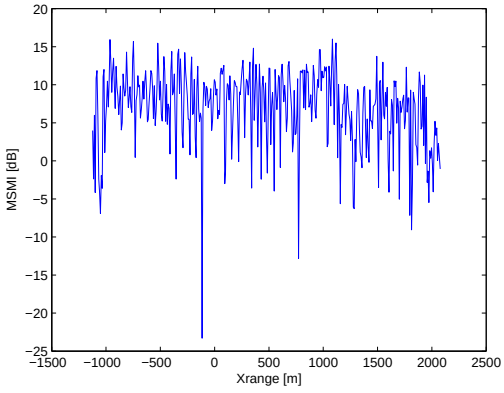

Figure 11: MSMI statistic along the transverse X-direction. Includes interference.

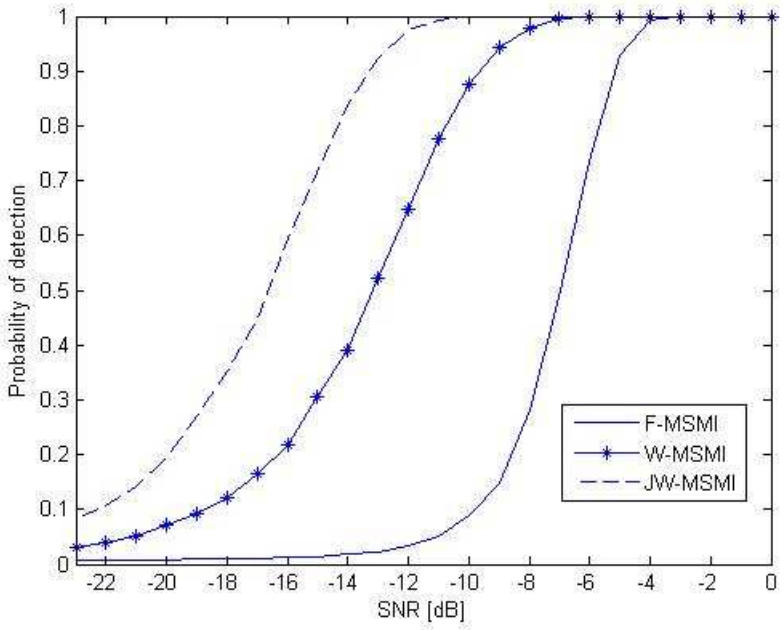

Figure 12: Probability of detection versus the SNR. The solid line represents the F-MSMI; the star-marked the W-MSMI; the dashed one the JW-MSMI.

the waveform diversity model in (32) as **W-MSMI** (Waveform MSMI) and the last one obtained introducing the JDL algorithm in (48) as **JW-MSMI** (JDL Waveform MSMI).

Figure 12 shows the probabilities of detection versus the signal to noise ratio (SNR) achievable with the three decision statistics. The solid line represents the probability of detection of F-MSMI, the ones marked with $\star$ the probability of detection of W-MSMI and the dashed line the probability of detection of JW-MSMI. The significant improvement achievable with the JDL algorithm is clearly evident. The JW-MSMI outperforms the others and the W-MSMI is better than the F-MSMI. In particular, for probability of detection equal to 0.9 the performance gain between JW-MSMI and W-MSMI is approximately 4 dB and approximately 8 dB between JW-MSMI and F-MSMI. The behavior of the curves highlights that the range dependency of the covariance matrix limits the achievable performance. It is remarkable that the gain between JW-MSMI and W-MSMI is achieved with dimension reduction; in fact, the dimension of the steering vectors is 27 in the space-time domain and 9 in the angle-Doppler domain. It is evident that all the statistics need a low SINR to achieve a good probability of detection; the distributed aperture radars use all the incoming signals and for this reason the needed SINR is lower than the one in a monostatic or bistatic radar.

6 Conclusions

In this paper we have considered the design and the analysis of a time-orthogonal waveform diversity model for distributed aperture radars. The signal model uses waveform diversity applied to distributed aperture radars; the chosen signals have different pulse durations and they do not overlap in time to achieve respectively waveform diversity and time-orthogonality. The orthogonality allows us to treat the signals at each receiver independently, simplifying the decision statistic. Based on the realization that both target and interference sources are in the near-field of the antenna array, this paper uses a data model based on true time delays. Furthermore, due to the relative motion between clutter and antennas, the clutter is not stationary. We account for this range dependency of the interference sources in the adaptive processing by converting the data from space-time domain to angle-Doppler domain based on the Joint Domain Localized (JDL) algorithm.

The detection capability of the new receiver is very good in the radial direction, where the MSMI statistic shows a narrow and high lobe centered at the target range, while in the transverse direction the system shows a performance decay due to a test statistic with high grating lobes. This is inherent to any single-frequency approach. The signaling scheme counteracts the grating lobes for many values of the range, but it is very asymmetric due to the range dependency of the interference. The probabilities of detection, analyzed through Monte-Carlo techniques, show that the JDL processor outperforms the one based on frequency diversity; furthermore, they show also the influence of the range dependency of the interference covariance matrix; the performance is significantly improved taking this non-stationarity into account.

The overall system is based on the orthogonality of the waves. It is interesting to analyze the effect of the loss of the orthogonality. It is evident that the estimated covariance matrix is no more block-diagonal and that some terms are different from zero outside of the principal diagonal. We did not account for this analysis in this work, but it is an interesting point of view for future developments. Another possible future research track might concern the analysis of a new waveform diversity model. In our analysis, we differentiated the signals only on the pulse duration. We expect an improvement in the system performances differentiating the signals on more parameters at the same time (like, for example, the pulse duration and the PRI) or using different shapes for the pulses.

Acknowledgement

We would like to thank Dr. Antonio De Maio of Università degli Studi di Napoli "Federico II" for his helpful comments on this work.

References

[1] B. Chen, L. Tong, and P. Varshney, "Channel aware distributed detection in wireless sensor networks," *IEEE Signal Processing Mag.*, pp. 16–26, July 2006.

[2] L. Applebaum and R. S. Adve, "Adaptive processing with frequency diverse distributed apertures," in *Proc. of the 2nd International Waveform Diversity and Design Conf.*, Jan. 2006. Kauai, HI.

[3] R. S. Adve, R. A. Schneible, and R. McMillan, "Adaptive space/frequency processing for distributed apertures," in *Proc. of 2003 IEEE Radar Conference*, May 2003. Huntsville, AL.

[4] P. Antonik and M. C. Wicks, "Waveform diversity: Past, present and future," in *Proceedings of the 2007 IET International Conference on Radar Systems*, Oct. 2007. Edimburgh, Scotlad.

[5] E. Fishler, A. Haimovich, R. Blum, D. Chizhik, L. Cimini, and R. A. Valenzuela, "MIMO radar: An idea whose time has come," in *Proceedings of the 2004 IEEE Radar Conference*, May 2004.

[6] N. J. Willis, *Bistatic Radar*. Technology Service Corporation, 1995.

[7] G. J. Frazer, Y. I. Abramovich, and B. A. Johnson, "Use of adaptive non-causal transmit beamforming in othr: Experimental results," in *Proceedings of 2008 International Conference on Radar*, Sept. 2008.

[8] D. Madurasinghe and L. Teng, "Adaptive array processing near field experiment," Tech. Rep. DSTO-TR-0361, Defense Science and Technology Organization, 1996.

[9] S. Sira, A. Papandreou-Suppappola, and D. Morrell, "Time-varying waveform selection and configuration for agile sensors in tracking applications," in *Proc. of the 2005 Int. Conf. on Acoustics, Speech and Signal Processing*, Mar. 2005.

[10] J. Ward, "Space-time adaptive processing for airborne radar," Tech. Rep. F19628-95-C-0002, MIT Linclon Laboratory, December 1994.

[11] B. Himed, J. H. Michels, and Y. Zhang, "Bistatic STAP performance analysis in radar applications," in *Proc. of the 2001 IEEE Radar Conference*, 2001. Atlanta, GA.

[12] P. K. Sanyal, R. D. Brown, M. O. Little, R. A. Schneible, and M. C. Wicks, "Space-time adaptive processing bistatic airborne radar," in *Proc. of the 1999 IEEE Radar Conference*, 1999. Waltham, MA.

[13] T. A. Winchester, "Pulsed radar return from a chaff cloud," *IEE Proceedings F, Radar and Signal Processing*, vol. 139, No.4, pp. 315–320, Aug. 1992.

[14] W. Melvin, M. Callahan, and M. Wicks, "Adaptive clutter cancellation in bistatic radar," in *Proc. of the 34th Asilomar Conference on Signals, Systems and Computers*, Nov. 2000.

[15] E. Lock and R. S. Adve, "Varying FM rates in adaptive processing for distributed radar apertures," in *Proc. of the 3rd International Waveform Diversity and Design Conf.*, June 2007. Pisa, Italy.

[16] H. Wang and L. Cai, "On adaptive spatial-temporal processing for airborne surveillance radar systems," *IEEE Transactions on Aerospace and Electronic Systems*, vol. 30, pp. 660–699, July 1994.

[17] R. S. Adve, R. A. Schneible, M. C. Wicks, and P. A. Antonik, "Waveform-space-time adaptive processing for distributed aperture radars," in *Proceedings of the 2005 IEEE International Radar Conference*, May 2005. Washington, DC.

[18] E. Kelly, "An adaptive detection algorithm," *IEEE Transactions on Aerospace and Electronic Systems*, vol. 22, No. 1, pp. 115–127, Mar. 1986.

[19] F. C. Robey, D. R. Fuhrmann, E. J. Kelly, and R. Nitzberg, "A CFAR adaptive matched filter detector," *IEEE Transactions on Aerospace and Electronic Systems*, vol. 28, pp. 208–216, January 1992.

[20] I. S. Reed, J. Mallett, and L. Brennan, "Rapid convergence rate in adaptive arrays," *IEEE Transactions on Aerospace and Electronic Systems*, vol. 10, No. 6, pp. 853–863, Nov. 1974.

[21] H. Wang and L. Cai, "On adaptive implementation of optimum mti in severly non-homogenous environments," in *Proc. of the IEEE Int. Radar Conf.*, May 1990.

[22] H. Wang and L. Cai, "A localized adaptive MTD processor," *IEEE Transactions on Aerospace and Electronic Systems*, vol. 27, pp. 532–539, May 1991.

[23] R. S. Adve, T. B. Hale, and M. C. Wicks, "Joint domain localized adaptive processing in homogeneous and non-homogeneous environments. part I: Homogeneous environments," *IEE Proc. on Radar Sonar and Navig.*, vol. 147, pp. 57–65, April 2000.

[24] M. Greco, F. Gini, and M. Diani, "Cfar detection of random signals in compound-gaussian clutter plus thermal noise," *IEE Proceedings on Radar, Sonar and Navigation*, vol. 148, no. 4, pp. 227–232, 2001.

[25] N. Goodman and D.Bruyere, "Optimum and decentralized detection for multistatic airborne radar," *IEEE Trans. on Aero. and Elec. Sys.* To appear, available at http://www.ece.arizona.edu/~ goodman/publications.htm.

[26] E. Lock and R. Adve, "Orthogonal frequency division multiplexing in distributed radar apertures," in *Proc. of the IEEE Radar Conf.*, May 2008. To appear.